

Article

Experimental Analysis of the Current Sensor Fault Detection Mechanism Based on Neural Networks in the PMSM Drive System

Kamila Jankowska  and Mateusz Dybkowski * 

Department of Electrical Machines, Drives and Measurements, Wrocław University of Science and Technology, 50-370 Wrocław, Poland

* Correspondence: mateusz.dybkowski@pwr.edu.pl

Abstract: In this paper, a current sensor fault detection mechanism based on multilayer perceptron (MLP) in a permanent magnet synchronous motor (PMSM) drive system is presented. The solution for the PMSM was previously described and tested only in simulation studies. The described application allows the detection of basic faults (lack of signal, gain error, signal noise) in current sensors and the indication of the phase (A or B) in which the fault occurred. The work is focused on the analysis of the fault detector but also presents the possibilities of their classification. The work mainly presents experimental research for different values of speed during the load and regenerative mode. In addition to the study of various operating conditions of the drive system, the detector efficiency was also verified for three neural structures with a different number of neurons in the hidden layers. The work also presents simulation tests (in Matlab Simulink software) for the additional conditions of the drive system for the same neural structures as in the experimental studies. The results obtained during offline and online faults detection with the use of the DS1103 controller are presented.

Keywords: current sensors; fault detection; neural detector; PMSM



Citation: Jankowska, K.; Dybkowski, M. Experimental Analysis of the Current Sensor Fault Detection Mechanism Based on Neural Networks in the PMSM Drive System. *Electronics* **2023**, *12*, 1170. <https://doi.org/10.3390/electronics12051170>

Academic Editor: Davide Astolfi

Received: 27 January 2023

Revised: 21 February 2023

Accepted: 27 February 2023

Published: 28 February 2023



Copyright: © 2023 by the authors. Licensee MDPI, Basel, Switzerland. This article is an open access article distributed under the terms and conditions of the Creative Commons Attribution (CC BY) license (<https://creativecommons.org/licenses/by/4.0/>).

1. Introduction

Fault detection in electric motor drive systems is becoming an increasingly popular research topic due to the use of electric motors in advanced systems that require an increased level of safety. Scientists use modern signal processing methods or artificial intelligence to detect as many failures as possible in the shortest possible time—at an early stage of damage [1–3].

Damage in drive systems is divided into three basic groups: motor damage, frequency converter damage, and measuring sensor damage [4]. In the literature, most works present the detection of electrical and mechanical faults in the electric motor itself [5–8]. The works present advanced detection methods based on artificial intelligence [9,10], object models [11–13], and measurement signals [14,15]; most of them use signals from measurement sensors. Despite the use of measuring sensors in the detection of other types of damage, there are fewer works dealing with their fault detection. In addition, the diagnostics of damage to measuring sensors offer great compensation opportunities (in respect of hardware and software), where so-called fault-tolerant control systems (FTCS) are applied there. In the case of other damage (e.g., to motor components) it is necessary to stop the system and replace the damaged component.

In drive systems, Hall-effect sensors are usually used to measure the current. The main advantage of this type of sensor is its non-invasive measurement. Damage in such a sensor may be caused by the corrosion of the core, changes in the magnetic properties of the ferrite core due to temperature, or, for example, changes in the orientation of the magnetic field induced in the sensor [16]. These damages can lead to a complete break of the sensor and loss of measurement signal or less significant failures (e.g., phase shift,

signal noise, and gain changes). Depending on the type of failure, as a result, the operating properties of the drive system may deteriorate, or the control stability may be completely lost. Therefore, fault detection of current sensors is an important issue.

In the literature, two types of methods for detecting faults in current sensors are mainly found; methods based on measurement signals and the object model. An example of work based on measurement signals may be the article [17], in which the authors presented the detection and location of faults in current sensors. The detector compared average normalized values of the phase currents in three phases. Damage detection was similarly described in [18], which detected two types of failures: signal loss and current abrupt. These are failures in which the current value significantly differs from the expected one. Paper [4] describes the application of a current tracking algorithm for the detection of signal loss of one or two sensors based on three-phase current and speed measurements. The algorithm presented in the work also allowed for detecting minor failures such as offset and gain errors. Each type of failure required a separate algorithm to recognize it. Detection was also carried out separately for each sensor, and appropriate indicators were determined for each sensor and failure type. Exceeding the threshold of 0.3 indicates a failure. The work of the drive system in the article was shown for less than 2000 rpm speed value, and some of the indicators almost reached the threshold value in a non-damaged state; detection for low-speed and dynamic states was not shown. The detection time varied between 0.02–0.03 s, and the use of neural networks allowed the shortening of this time.

Apart from using current measurement, there are also several papers in the literature where the detection of current sensor faults is performed by measuring and estimating the dc-link current in the intermediate circuit [14,19,20]; however, these articles only presented simulation results. The operation of the detector under variable operating conditions of the drive system or various types of failures was also not shown.

Current sensor fault detection applications are mainly based on state variable observers. For this purpose, different types of observers are used—SMO (sliding mode observer) [11,21], EKF (extended Kalman filter) [22], nonlinear observer [23], and LO (Luengerberger observer) [24]. Detection is carried out by comparing the observed value with a measured value of current. When the difference between them exceeds a certain value, the detector indicates that a fault has occurred. Algorithms of this type make it possible to indicate a damaged phase, but they are strongly dependent on motor parameters. The quality of the estimation is also influenced by the speed and load of the motor.

Several works have presented the detection of current sensor damage using methods based on artificial intelligence (AI). Those papers describe the detection of an induction motor [25–27]; such a solution for PMSM has been described only in simulation studies by the authors of this work [28].

In the case of articles [25,26], only the detection and location of faults without their classification were presented. In this case, signal loss detection times were below 1 ms, but for other types of failures, even several seconds. However, in [27], the neural network (NN) was used only for fault classification, and the current estimator was responsible for the detection. The presented solution correctly classifies the failure only after its compensation. This application is not resistant to errors resulting from the impact of sensor failure on the entire control structure. The results were also shown only for stable operating conditions, and the operation of the network in the regenerative mode was not shown. Classification time also varied between 0.02–0.05 s and the paper showed only simulation results.

These are the basic elements that distinguish existing works in the literature from the presented solution. This article presents both the detection and classification of faults in simulation and experimental studies. Besides, the proposed application does not require additional current estimators for detection. In addition, the neural networks described in previous works have different structures and input and output vectors.

The advantage of the presented work on methods based on the object model is that using a neural network does not require prior knowledge of the research object. There is no need to know the motor parameters, which can be difficult to determine with high precision.

Additional motor parameters may change over time. However, usually, in the case of signal methods, only fault detection is presented without their classification. Individual works, which show the determination of the type of failure using signal methods, require separate algorithms for each type of failure and each of the sensors. Works based on signal methods show the detection of signal loss, offset, and variable gain. Each of these failures gives effects that can be described by appropriate equations. There is no distinction between measurement noise and variable gain, which show similar symptoms and require analysis of the signal image in several samples.

This paper presents an analysis of the fault detection system based on neural networks in a vector-controlled permanent magnet synchronous motor (PMSM). So far, neural networks have found many applications in drive systems with electric motors (motor damage detection [29], neural controllers [30], motor parameters identification [31], and estimation of state variables [32]) and have allowed for high efficiency. However, the solution presented in this article has not yet been described in the literature for the PMSM drive system. The article presents simulation and experimental results and is an extension of the author's work [28], which presented only simulation studies. A special difference between the previous paper is the expansion of the input vector with the value of the stator current from the previous samples. The input vector from simulation studies turned out to be insufficient in experimental tests. In the presented work, it was possible to obtain enough high efficiency for the same neural structure and training method as in previous simulation studies.

The neural detector described in the paper indicates three main types of faults: signal loss, gain error, and measurement noise. The detector efficiency was verified for different values of speed, motor load, regenerative mode, and three neural network structures. In addition to detection, the failure is also localized (the detector indicates a damaged phase), which makes it possible to compensate for it. In this paper, fault detection during operation in regenerative mode was also taken into account, which is usually omitted in papers presenting fault detection of current sensors. Detection is based on the multilayer perceptron (MLP) and raw signals without the use of advanced signal processing methods, which results in a low computational complexity of the solution. It was decided to use MLP due to its high efficiency in relevant problems of damage classification [29,33–35]. In addition, the implementation possibilities of the perceptron or similar neural structures on microcontrollers have been repeatedly presented in the literature, which shows the possibilities of using the detector in industrial practice [36–38]. The paper also presents the possibilities of damage classification (indication of one of the three analyzed failure types) with the use of MLP; fault classification is based on the same input vector as the fault detector, excluding the regenerative mode, and the classifier recognizes the same three types of damage. The research was carried out in Matlab/Simulink and dSpace environments with the use of a DS1103 controller. In the research, the location and classification of damage are shown without fault compensation. The lack of compensation affects the entire control structure, which makes the correct location and classification of failures more complicated. However, such an approach means that additional tools, such as estimators sensitive to changes in motor parameters, are not required to perform correct detection. The work is supplemented by simulation studies conducted for the same neural structures in Matlab/Simulink. It is also worth emphasizing that only two current sensors were used in the presented solution, which is in line with industrial solutions.

The work is divided into five parts. The first part presents the motivation to undertake research and its innovativeness, followed by the theoretical basis of the developed neural detector based on the MLP NN. The third part shows the control structure used in the research in simulation and experimental tests and the significance of the research undertaken. Simulation results for fault detection are described in the fourth chapter. The fifth chapter contains experimental results and verification of the effectiveness of the fault detector and fault classifier. Both in simulation and experimental studies, the results for offline and online detection are presented. The last part presents a summary of the work.

2. Neural Detector—Structure Features

The fault detection mechanism presented in this paper is based on a multilayer perceptron. The perceptron is a feedforward neural network consisting of an input layer, n -hidden layers, and an output layer. Each neuron in each layer is connected to a neuron in the next layer; there are no connections between the neurons of the same layer [39,40].

The operation of this type of Neural Network can be written simply by the equation [29]:

$$y_k = f_3 \left(f_2 \left(\sum_{i=1}^M w_{ki}^{(2)} \times f_1 \left(\sum_{j=1}^N w_{ij}^{(1)} \times x_j + w_0^{(1)} \right) + w_0^{(2)} \right) + w_0^{(3)} \right) \quad (1)$$

where

y_k — k -th output of the network,
 x_j — j -th input of the network,
 $w_{ij}^{(1)}, w_{ki}^{(2)}$ —weights of the first and second hidden layers, respectively,
 $w_0^{(1)}, w_0^{(2)}, w_0^{(3)}$ —biases in the first and second hidden layers, and output layer, respectively,
 f_1, f_2, f_3 —activation functions of the first hidden layer, second hidden layer, and output layer, respectively.

MLP performs global approximation, i.e., individual elements of the input vector are processed by many neurons simultaneously. The training process consists in modifying the network weights in such a way as to minimize the mean square error (MSE)—the objective function of the output and expected values. The Levenberg–Marquardt training method with Bayesian regularization, was used in the study. Regularization introduces a change to the objective function. Not only is the aim to minimize the mean square error but also to achieve it with the lowest possible weights [41].

The paper presents a study of a fault detector, which indicates faulty phase (A or B), and a fault classifier, which also defines the type of failure. Three types of neural structures, with a different number of neurons in hidden layers for fault detectors, are tested. In the case of the classifier, the results are presented only for one neural structure. The Levenberg–Marquardt training method with Bayesian regularization, logistic function as activation functions in hidden layers, and linear function as an output layer activation function were chosen as constant parameters.

The main part of designing a neural detector is the selection of the input vector. The most important elements of the input vector are the currents in phases A and B, from the current and previous samples. Using samples from previous measurements allows to create a more complete picture of the signal for the neural detector and the recognition of faults that do not directly indicate faults in every measured sample. Another important signal is the 0–1 $\Delta i_{s\alpha\beta}$ result of comparing the values of the stator current components α - β determine based on measurements from sensors in different phases.

In the field-oriented control structure, the measured currents in the ABC frame are converted to the stationary α - β frame. Measurement in three phases or two can be used for this transformation. This gives three possibilities to determine $i_{s\alpha}$ and $i_{s\beta}$, using the following equations:

$$i_{s\alpha 1} = \frac{2}{3}(i_{sA} - \frac{1}{2}(i_{sB} + i_{sC})), i_{s\beta 1} = \frac{\sqrt{3}}{3}(i_{sB} - i_{sC}), \quad (2)$$

$$i_{s\alpha 2} = i_{sA}, i_{s\beta 2} = \frac{\sqrt{3}}{3}(i_{sA} + 2i_{sB}), \quad (3)$$

$$i_{s\alpha 3} = -(i_{sB} + i_{sC}), i_{s\beta 3} = -\frac{\sqrt{3}}{3}(i_{sB} - i_{sC}), \quad (4)$$

In the absence of a fault, these currents are almost equal to each other. When a fault occurs in any of the phases, discrepancies in them appear. Then the 0–1 signal $\Delta i_{s\alpha\beta}$ is set

to 1. In the control structure, α - β currents are determined on the basis of Equation 3. Due to only two current sensors in the control structure being used in the work, the value of I_{sC} was determined on the basis of delivery I_{sA} and I_{sB} by the following equation:

$$i_{sC} = -i_{sA} - i_{sB}, \tag{5}$$

As the correct current values are dependent on the speed value, the reference speed ω_{ref} is also supplied to the detector input. Currents in the d - q axis in the rotor system and the space vector module $|I_S|$ were used as auxiliary symptoms. The full input vector is presented below:

$$\begin{bmatrix} i_{sA}(k), & i_{sA}(k-1), & i_{sA}(k-3), & i_{sA}(k-5), & i_{sA}(k-7), \\ i_{sB}(k), & i_{sB}(k-1), & i_{sB}(k-3), & i_{sB}(k-5), & i_{sB}(k-7), \\ \omega_{ref}, & \Delta i_{s\alpha\beta}, & |I_S|, & i_{sd}, & i_{sq} \end{bmatrix}^T, \tag{6}$$

A description of individual input vector signals is shown in Table 1.

Table 1. Individual inputs of the neural detector.

Input	Value	
$i_{sA}(k), i_{sA}(k-1), i_{sA}(k-3), i_{sA}(k-5), i_{sA}(k-7)$		i_{sA} —phase A current
$i_{sB}(k), i_{sB}(k-1), i_{sB}(k-3), i_{sB}(k-5), i_{sB}(k-7)$		i_{sB} —phase B current
ω_{ref}	ω_{ref}	ω_{ref} —reference value of speed
$ I_S $	$ I_S = \sqrt{i_{s\alpha}^2 + i_{s\beta}^2}$	$i_{s\alpha}, i_{s\beta}$ —stator current components
$\Delta i_{s\alpha\beta} [0\ 1]$	$i_{s\alpha 1} = i_{s\alpha 2} = i_{s\alpha 3} \wedge i_{s\beta 1} = i_{s\beta 2} = i_{s\beta 3}$	$\Delta i_{s\alpha\beta} = [0\ 1]$
i_{sq}	i_{sq}	i_{sq} —a calculated value of stator current component q axis in rotor frame
i_{sd}	i_{sd}	i_{sd} —a calculated value of stator current component d axis in rotor frame

The fault detector and the fault classifier are presented as two separate neural structures. The fault detector output is one element that can take the following values:

- 0—no fault,
- 1—faulty sensor in phase A,
- 2—faulty sensor on phase B.

The design of the fault classifier is carried out in the same way; the fundamental difference is the number of outputs. The first output of the fault classifier defines phase A, the second defines phase B. For both outputs, the values represent the following faults:

- 0—no fault,
- 1—signal loss,
- 2—signal noise,
- 3—gain error.

In addition, the classifier required more neurons in the first hidden layer. The same neural structures were used in both experimental and simulation studies.

3. Control Basics in Simulation and Experimental Studies

This chapter describes the control algorithm used in the research and sample transients of current and speed. In the paper, the field-oriented control (FOC) structure was used for both simulation and experimental research. A current sensors fault detector, based on the neural network, has been added to the standard control structure. The complete control diagram is shown in Figure 1.

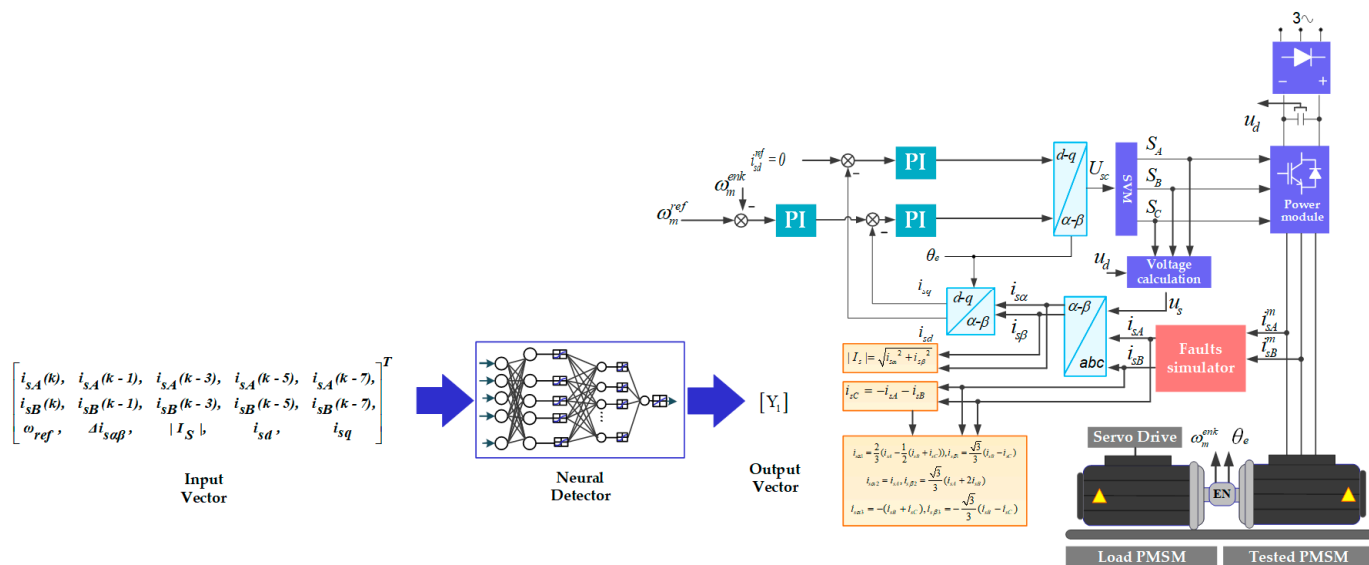


Figure 1. Diagram of control structure with neural detector used in simulation and experimental research.

Experimental tests were carried out on a 0.894 kW PMSM motor from Moog (G403-2007A). The essential parameters of the motor are presented in Table 2. The dSpace DS1103 controller with Control Desk software was used in the tests, the position of the shaft was measured with an incremental encoder (36,000 imp./rev), and the current measurement was carried out using LEM-type current transducers. Another Moog PMSM motor (G404-2009A—0.89 kW) controlled by a Moog servo drive was used as the load. Photos of the laboratory set-up are shown in Figure 2. A frequency converter with a switching frequency of 15 kHz was used to supply the tested motor. The sampling frequency in the studies was 1×10^{-4} s. The faults were simulated in a software manner. Table 3 shows the equations that were used to simulate the individual failures.

Table 2. Parameters of the tested motor in simulation and experimental research.

P_N [kW]	P_p [-]	n_N [rpm]	T_N [Nm]	I_N [A]	J [kg·m ²]	R_S [Ω]
0.894	4	6200	1.4	1.9	0.000039	4.6615



Figure 2. Photos of the experimental set-up.

Table 3. Considered fault types of current sensors.

Type of Fault	Current Value
Variable gain	$i_s^m = (1 - \gamma)i_a$
Noise	$i_s^m = i_a + n(t)$
Lack of signal	$i_s^m = 0$
Intermittent signal	$i_s^m = [0, 1]i_a$

where i_s^m —measured current, i_a —real current, $n(t)$ —white noise, γ —constant value from the range $\langle -1, 1 \rangle$.

Firstly, the operation of the PMSM drive during the failure of the stator current sensor was presented. The purpose of these studies is to show the impact of failure on the transients. Figure 3 shows the currents and speed error transients in normal operation—without damage and during damage to the current sensors in phase A and phase B in experimental tests.

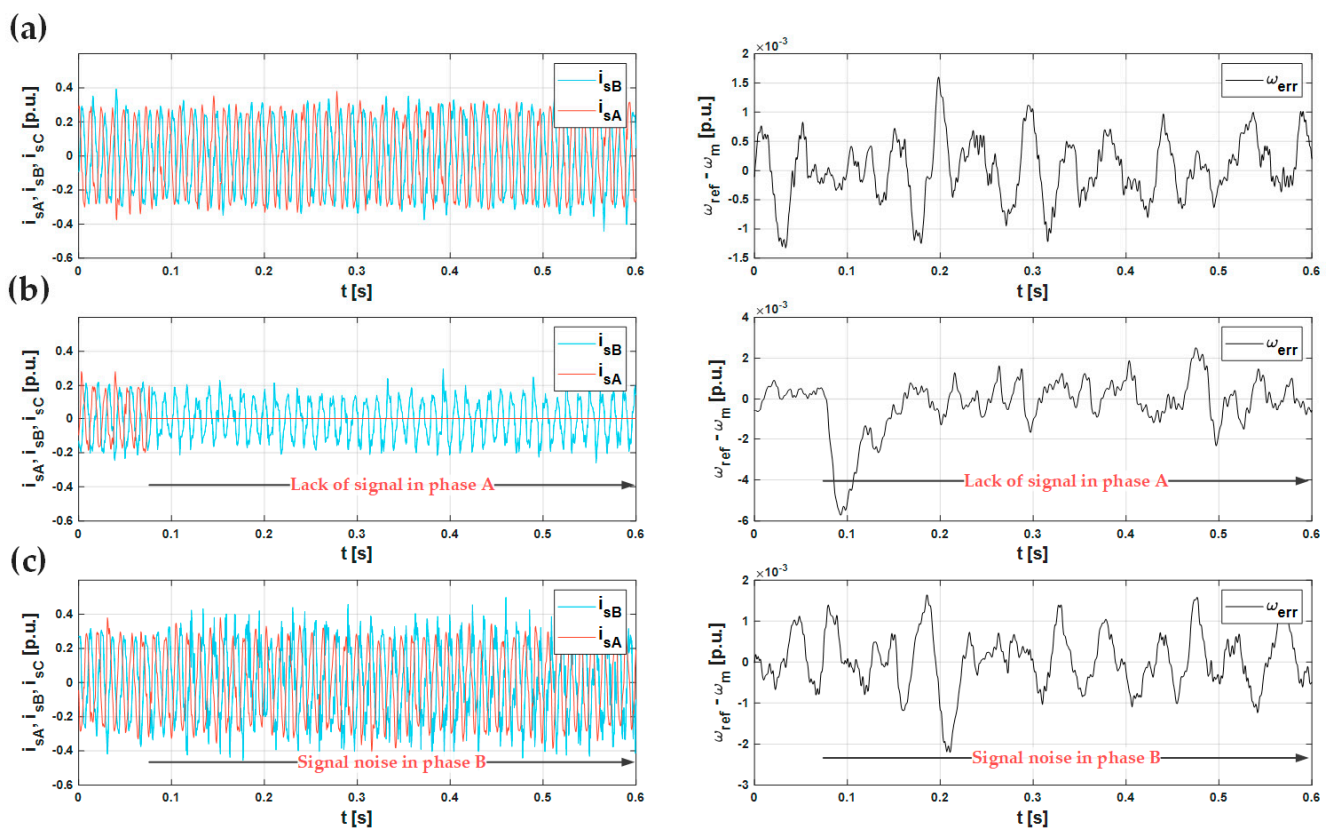


Figure 3. Transients of current and speed error during normal operation of the drive system (a), lack of signal in phase A (b), and signal noise in phase B (c) in experimental studies.

The impact of damage was visible primarily in the current transients. The speed error did not change much. Peaks in speed occurred at the early stage of damage appearance. Incorrect current measurement resulted in increased total harmonic distortion (THD) in the current transients, which is presented in Table 4. This confirms the impact of even small faults on the operation of the drive system and the importance of their detection.

Table 4. Total Harmonic Distortion.

Fault	THD(I _A)	THD(I _B)
No fault	1.12%	1.25%
Lack of signal in phase A	-	4.46%
Signal noise in phase B	1.9%	3.54%

Adequate transients for simulation tests are shown in Figure 4. In the simulation tests, a PMSM with the same parameters as in the experimental tests was used (Table 2). The model of the control structure was made in the Matlab Simulink (Sim Power System toolbox) [42] with a 15 kHz switching frequency; the neural network was designed using the Neural Network Toolbox [43]. In this research, the Euler method with a fixed step size equal to 1×10^{-5} s was used. The comparison of THD values is presented in Table 5. The simulation results, except for signal loss, were consistent with the experimental tests.

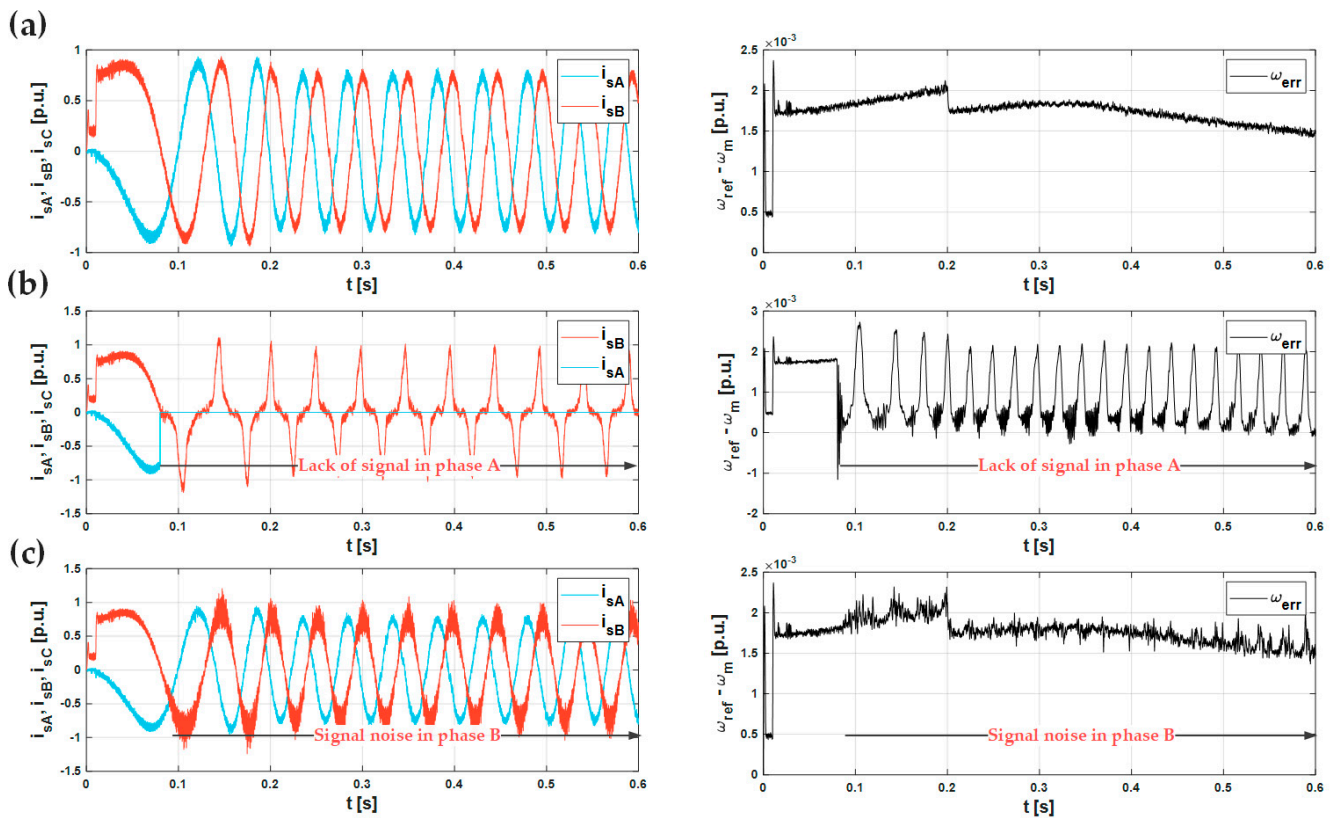


Figure 4. Transients of current and speed error during normal operation of the drive system (a), lack of signal in phase A (b), and signal loss in phase B (c) in simulation studies.

Table 5. Total Harmonic Distortion.

Fault	THD(I _A)	THD(I _B)
No fault	1.13%	1.27%
Lack of signal in phase A	-	56.88%
Signal noise in phase B	1.99%	2.51%

4. Fault Detection—Simulation Results

This chapter presents the simulation verification of the tested neural detector and classifier. Preparation of the neural detector and classifier in simulation studies is based on the following stages:

- (1) generating training data using Simulink;
- (2) training process using Neural Network Toolbox, selection of the neural structure and input signals in Matlab;
- (3) implementation of the neural structure along with the parameters obtained in the training process in the motor control algorithm in Simulink;
- (4) conducting online detection on the motor model in Simulink.

Statistical data are presented for neural detector performance analysis obtained by offline detection with raw signals. The exact parameters of the training and testing vectors are presented in Table 6.

Table 6. Parameters of training and testing vectors in simulation studies.

Feature	Training Data	Testing Data
Number of samples	1,560,002	1,560,002
Speed values	$\pm 0.2\omega_{ref}$, $\pm 0.5\omega_{ref}$, $\pm 0.8\omega_{ref}$	$\pm 0.3\omega_{ref}$, $\pm 0.6\omega_{ref}$, $\pm 0.9\omega_{ref}$

The damage detection results are presented for three neural structures using confusion matrixes in Figure 5. The results are obtained for the operation of the drive system during failures without their compensation.

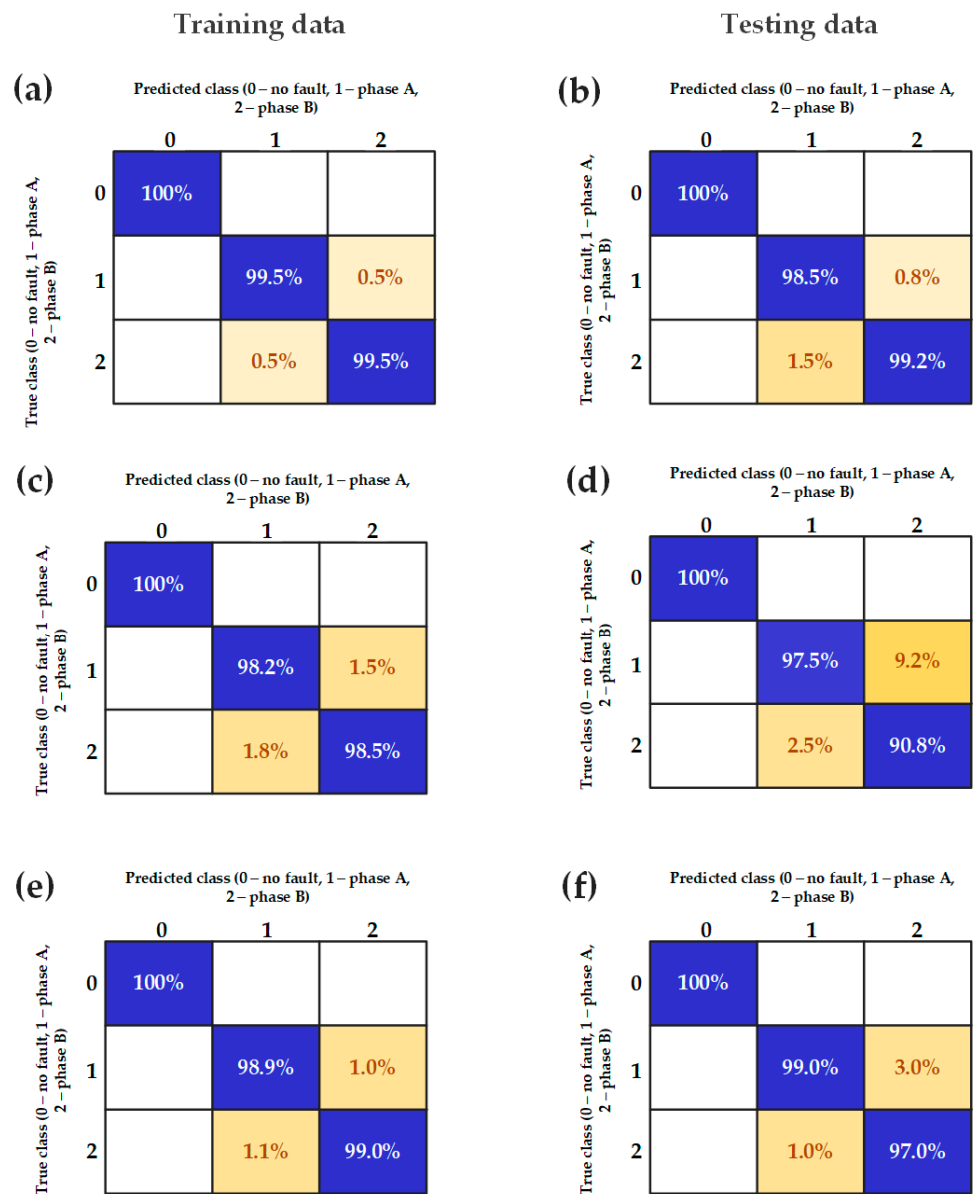


Figure 5. Confusion matrixes with percentage results for fault detector for training and testing data for tested structures 15-10-1 (a,b), 17-10-1 (c,d), and 20-10-1 (e,f) in simulation studies.

The obtained results indicate the lack of false alarms during fault detection, which is the essence of detection and developed systems.; errors are made only in indicating a damaged phase. Another element of the system is the classification of failures. The results for the classifier are also presented using the confusion matrixes (Figure 6). Both detection and classification systems can operate in parallel. This ensures the absence of false alarms by using a fault detector and determining the type of damage by using a classifier. Fault classification allows for determining fault severity.

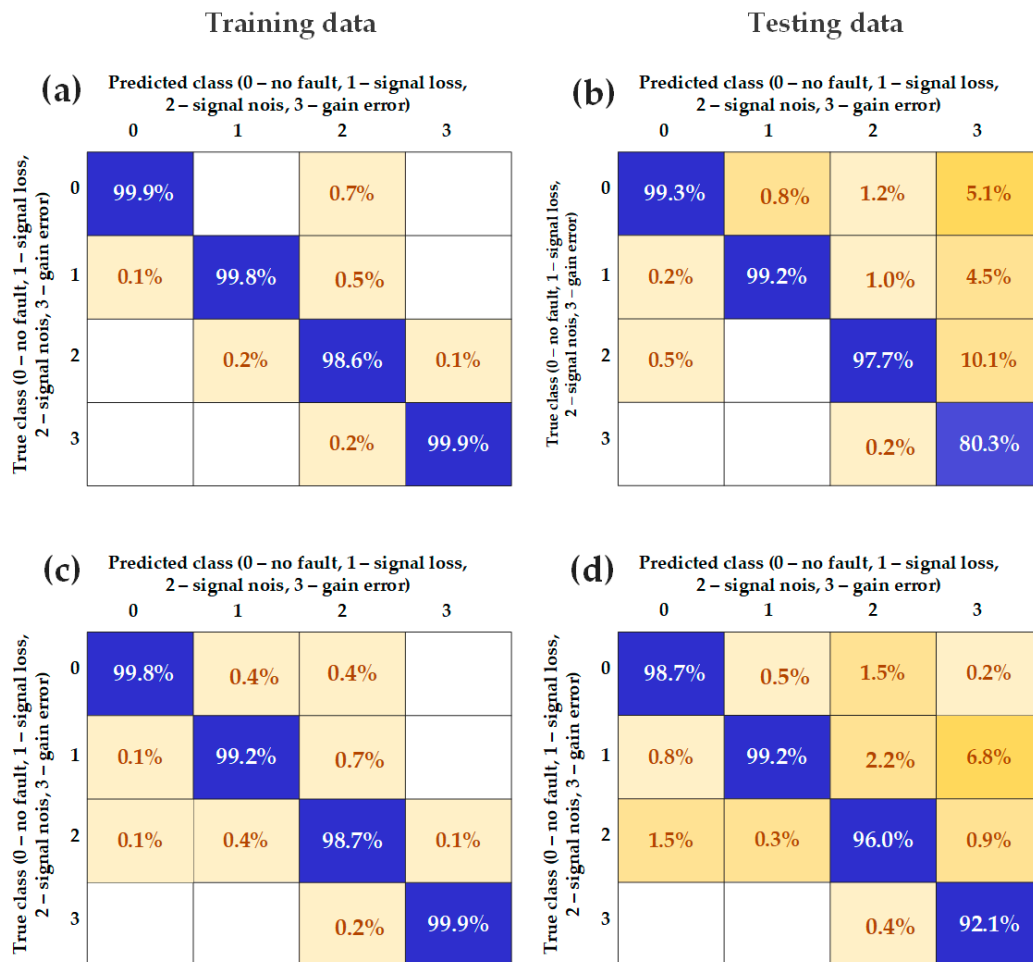


Figure 6. Confusion matrixes with percentage results for training and testing data for tested structure 30-10-2 for Output1(phase A) (a,b) and Output2(phase B) (c,d) in simulation studies.

In addition to the effectiveness, the influence of individual inputs of the neural detector on its output was also analyzed. For this purpose, Figure 7 shows the correlation of individual inputs with the output of the detector. The 0–1 $\Delta\alpha\beta$ signal and the B-phase current measurement have the greatest impact on the detector output.

Not all relevant aspects of the detector can be shown by percentage results. Sample transients for the operation of the detector and classifier during faults in phases A and B are shown in Figure 8. These results represent online detection after neural network implementation in Simulink. Ten samples of the output of the neural network were rounded and this was the response of the detector. The number of rounded samples results from the high sampling frequency. The online verification is presented for the detector structure, which achieved the highest efficiency—15-10-1 and 30-10-2 for the classifier.

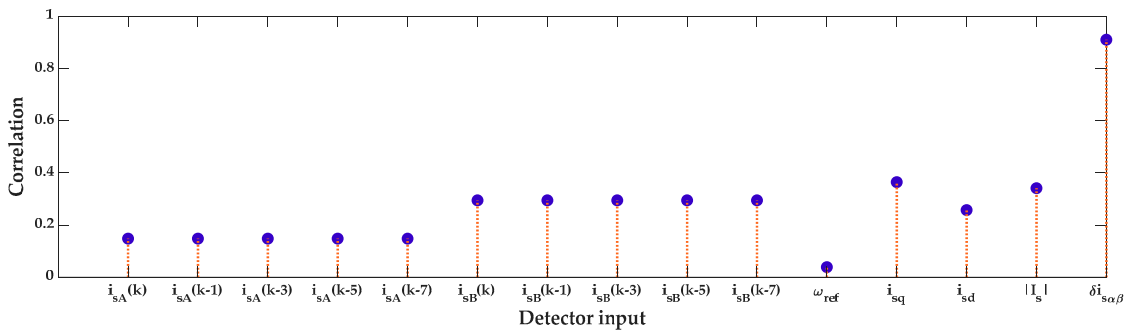


Figure 7. Correlation values between input vector elements and output vector in simulation studies.

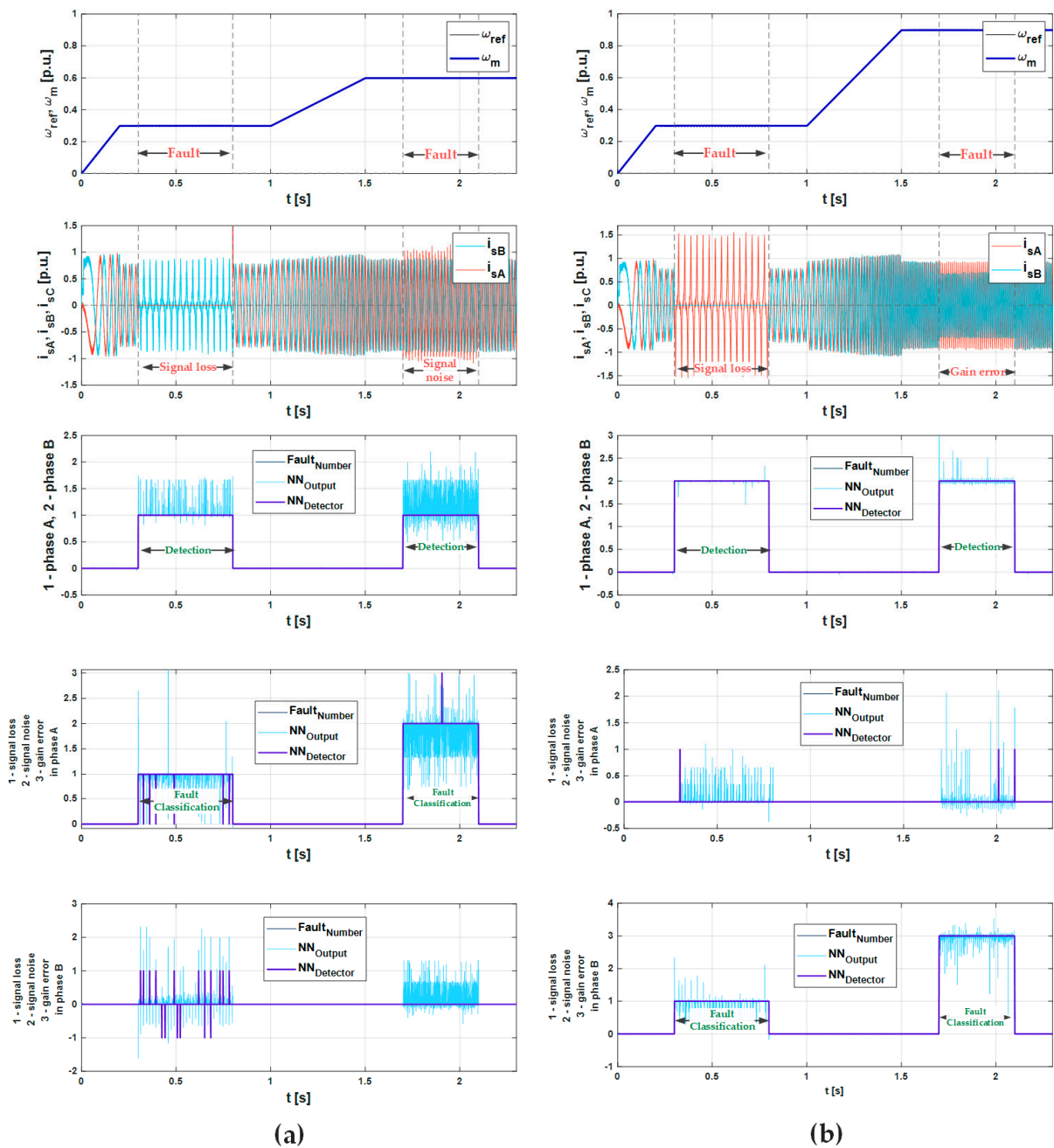


Figure 8. Transients of speed, currents, neural detector output, and neural classifier output1 and output 2 during faults in phases A (a) and B (b).

Based on the presented results, it can be concluded that signal noise is the most difficult failure to detect. The raw output of the network has the most oscillations. Significantly more oscillations also appear with failures in phase A. The most potential errors in classification may appear in the distinction between signal noise and gain error. Symptoms in many samples may be the same. In Figure 8a, the raw output of the phase A classifier shows the oscillation between these faults. For all cases, only classification errors appear, and damage detection is correct, which is consistent with the presented percentage results.

5. Fault Detection—Experimental Results

This chapter presents the experimental studies of the detector and the fault classifier. Preparation of the neural detector and classifier in experimental studies was based on the following stages:

- (1) carrying out measurements on experimental set-up with the use of Matlab/Simulink and dSpace software, and DS1103 controller, used as offline training and testing data;
- (2) the training process with the selection of the neural structure and input signals in Matlab with the use of Neural Network Toolbox;
- (3) implementation of the neural structure along with the parameters obtained in the learning process in the motor control algorithm in Simulink and dSpace software;
- (4) conducting online detection on a real-time DS1103 controller.

The full research process is shown in Figure 9.

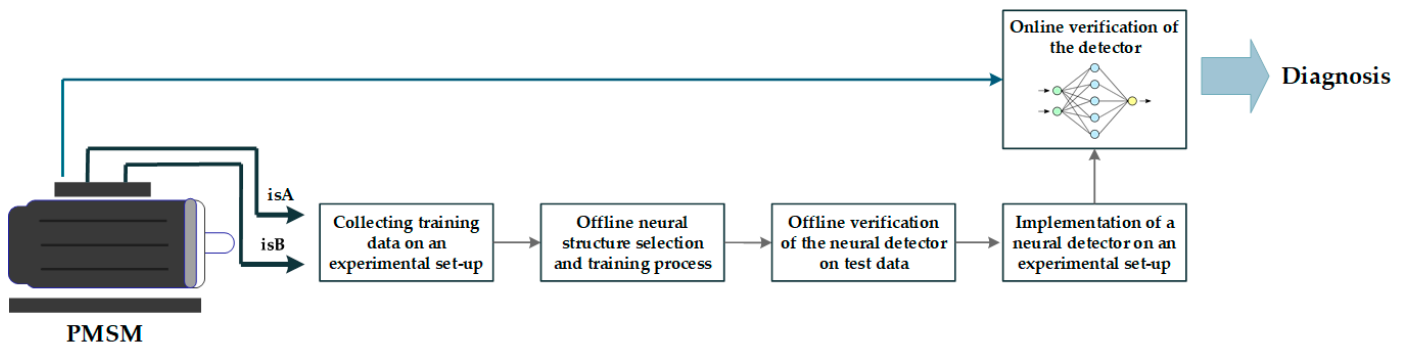


Figure 9. Correlation values between input vector elements and output vector in simulation studies.

To carry out online detection, a neural detector with parameters obtained in offline training was implemented in Simulink at the laboratory set-up.

Statistical data is presented for neural detector performance analysis obtained by offline detection. The exact parameters of the training and testing vectors are presented in Table 7.

Table 7. Parameters of training and testing vectors in experimental studies.

Feature	Training Data	Testing Data
Number of samples	380,010	228,006
Speed values	$\pm 0.1\omega_{ref}, \pm 0.2\omega_{ref}, \pm 0.3\omega_{ref}$	$\pm 0.075\omega_{ref}, \pm 0.15\omega_{ref}, \pm 0.225\omega_{ref}$
Load Values	$0.1 T_N, 0.3 T_N$	$0.2 T_N$
Regenerative mode	$0.1 T_N, 0.3 T_N$	$0.2 T_N$

For all presented neural structures, the training process was carried out for 550 epochs. A detailed verification of effectiveness is presented based on the confusion matrixes (Figure 10). The results are presented for both the training and testing data. Detection efficiency is presented as the ratio of samples of correct responses of the neural network to all measurement samples in the percentage form. In each case, the efficiency of failure

location is about 99%. In addition, these results show that failure detection is 100% for every structure, and this is the most important element of the developed solution.

Training data

Testing data

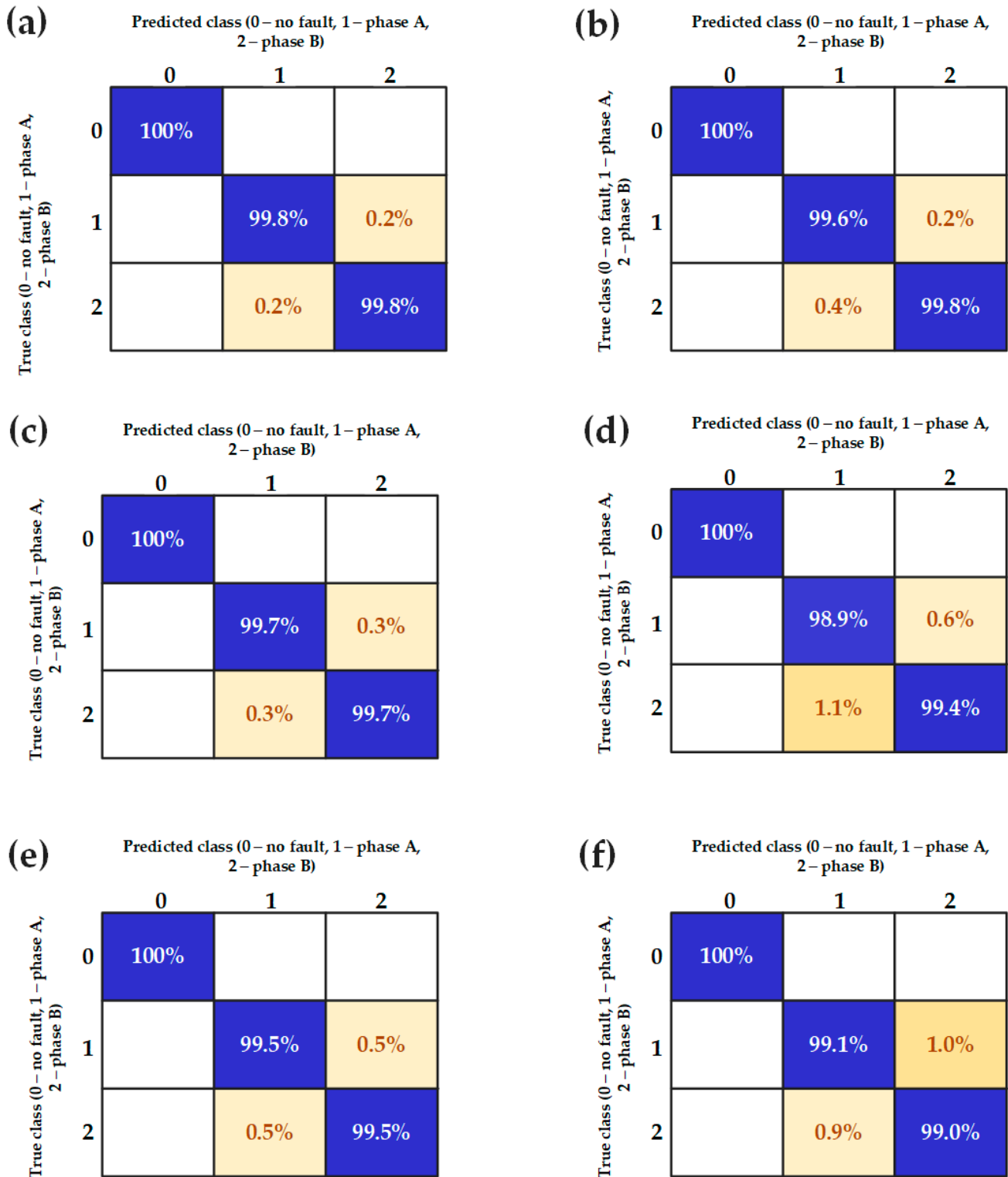


Figure 10. Confusion matrixes with percentage results for fault detector for training and testing data for tested structures 15-10-1 (a,b), 17-10-1 (c,d), and 20-10-1 (e,f) in experimental studies.

Based on Figure 10, it can be concluded that the 15-10-1 structure is the most effective of the studied structures. This is consistent with simulation studies.

The presented detector has an extended input vector (15 elements). However, these are signals readily available in the control structure. To prove that each of them is significant, the correlation values of individual inputs with the output vector for the tested detector are presented in Figure 11. The $0-1 \Delta i_{s\alpha\beta}$ signal shows the greatest connection with the output vector, while the others have a similar to each other effect. From the presented graph, it can also be concluded that the values of the samples from the current measurements in phase B are slightly more important in the detection of faults. Moreover, in the confusion matrixes, it can be seen that slightly more errors are made during the damage in phase A. The significance of the inputs in the detection is consistent with the simulation results.

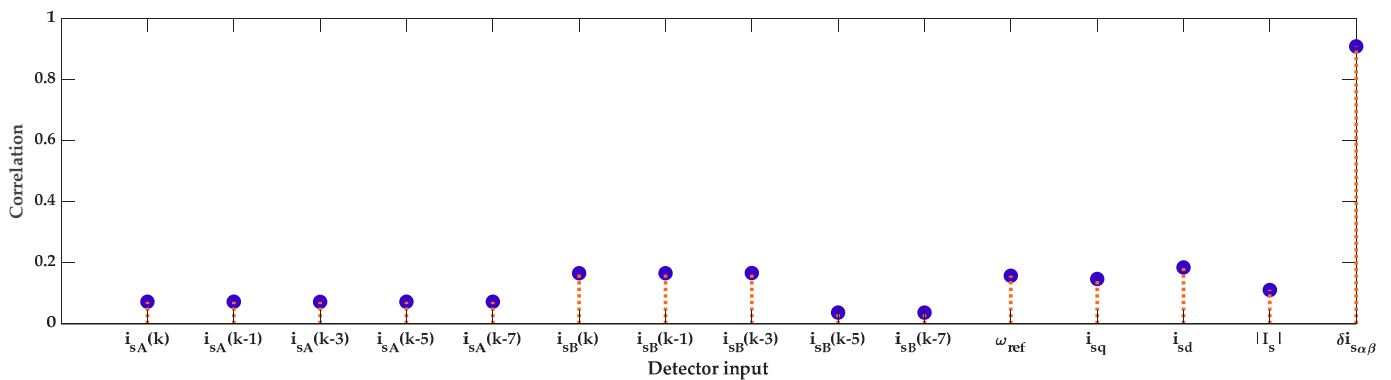


Figure 11. Correlation values between input vector elements and output vector.

The progress of a training process for individual neural structures is shown in Figure 12. To better illustrate the course of training errors, the results are presented on a logarithmic scale. The structure with the highest efficiency (15-10-1) obtained the smallest mean squared error (mse). The mse declined almost until about 500 epochs. The remaining structures have not improved their parameters since about 150 epochs of the training process. An increase in the number of neurons in the first hidden layer decreased the fit of the neural network.

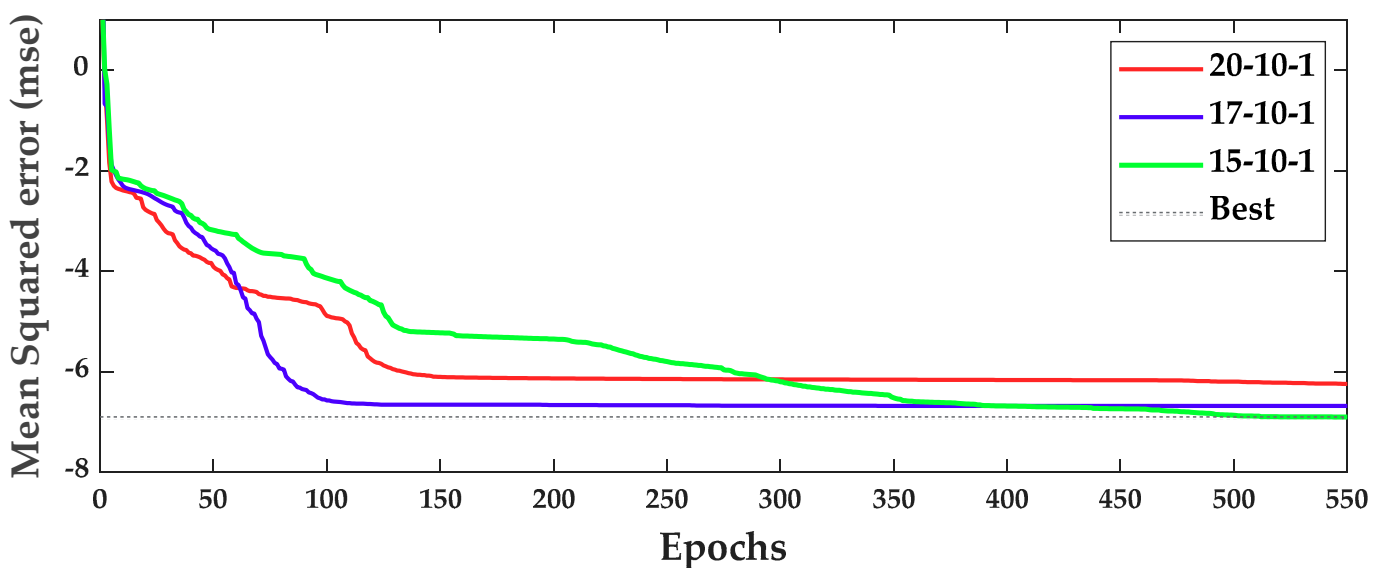


Figure 12. Mean squared error transients during the learning process for tested structures.

Online detection results are presented only for the NN structure that achieved the highest efficiency in offline detection analysis—10-15-1. The averaged and rounded value

from the current sample and the two previous samples are taken as the detector response ($NN_{Detector}$), which increases the detector’s resistance to making errors by single incorrect results of the neural network. The figure shows both the response of the raw neural network (NN_{Output}) and the response of the detector. Online detection was performed for the same range of speed and load values as listed in Table 7 for the test data. First, the results are presented for the detection of signal loss in the case of no-load operation (Figure 13).

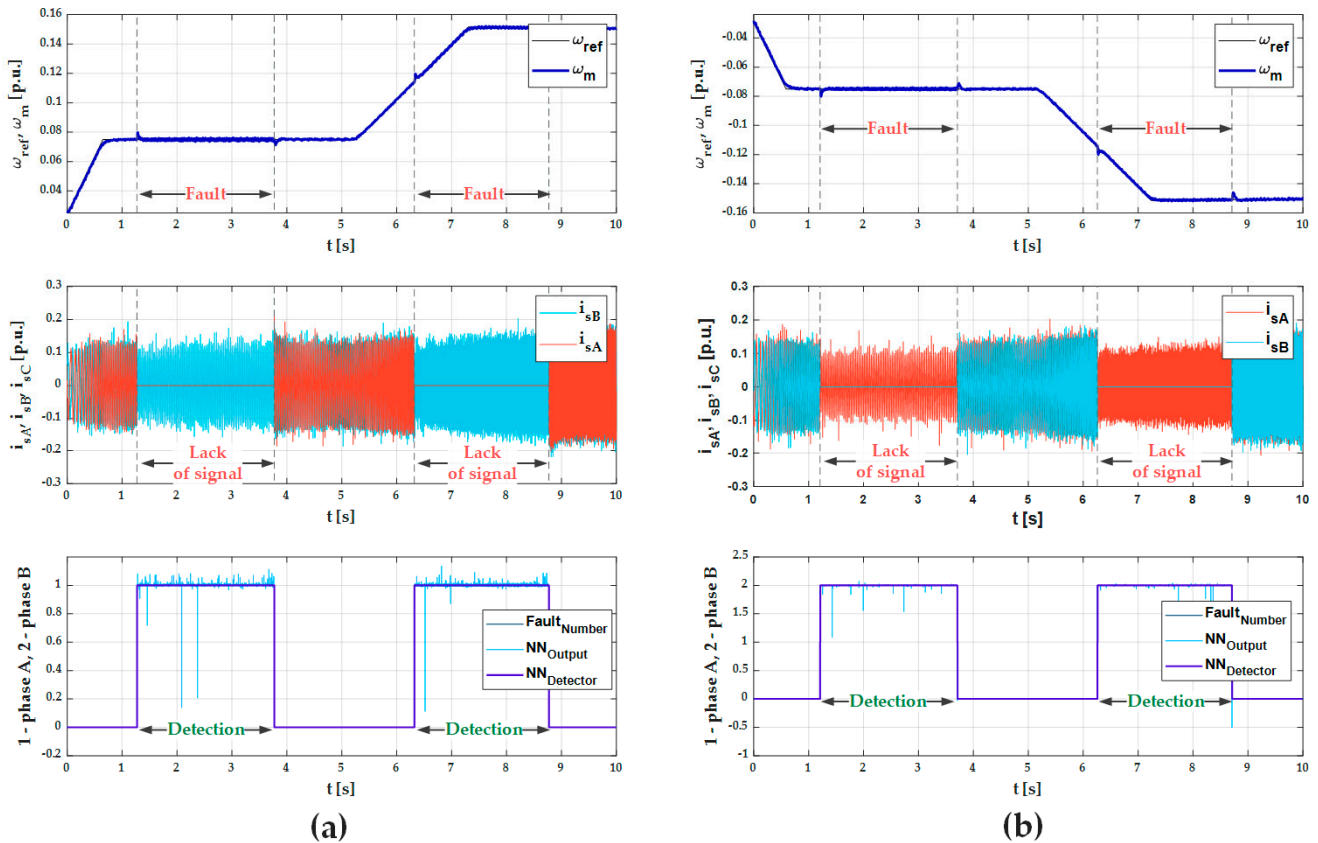


Figure 13. Transients of speed, stator currents, and detector response during lack of signal in phase A without load (a) and lack of signal in phase B without load (b).

Figure 13 shows the detector’s immunity to false alarms. The failure is correctly detected in the dynamic state, and the values even at the raw output of the network, are close to the expected result. As in the simulation results, the raw network output during a fault in phase B is closer to the expected value than during a fault in phase A.

Figure 14 shows the operation of the detector in load and regenerative mode in both directions. The detector showed high efficiency in both cases. However, during motor operation with a load, the raw signal from the neural network deviated more from the correct value than in no-load conditions. On the transients, it can also be observed that the detection proceeded correctly both during stable operation and dynamic states. Switching on the load or the regenerative mode during the failure also did not disturb the detection. The faulty phase was indicated correctly.

Signal loss is the easiest failure to detect because it most significantly affects the control structure. Other failures—gain error and measurement noise has little impact on it. Despite this, the detector detected and located failures with high efficiency. The results are shown in Figure 15 under load conditions. Based on Figure 15, it can be concluded that the detection of measurement noise caused the most errors in the neural detector response. However, these errors concern the determination of the damaged phase, and not the failure detection itself.

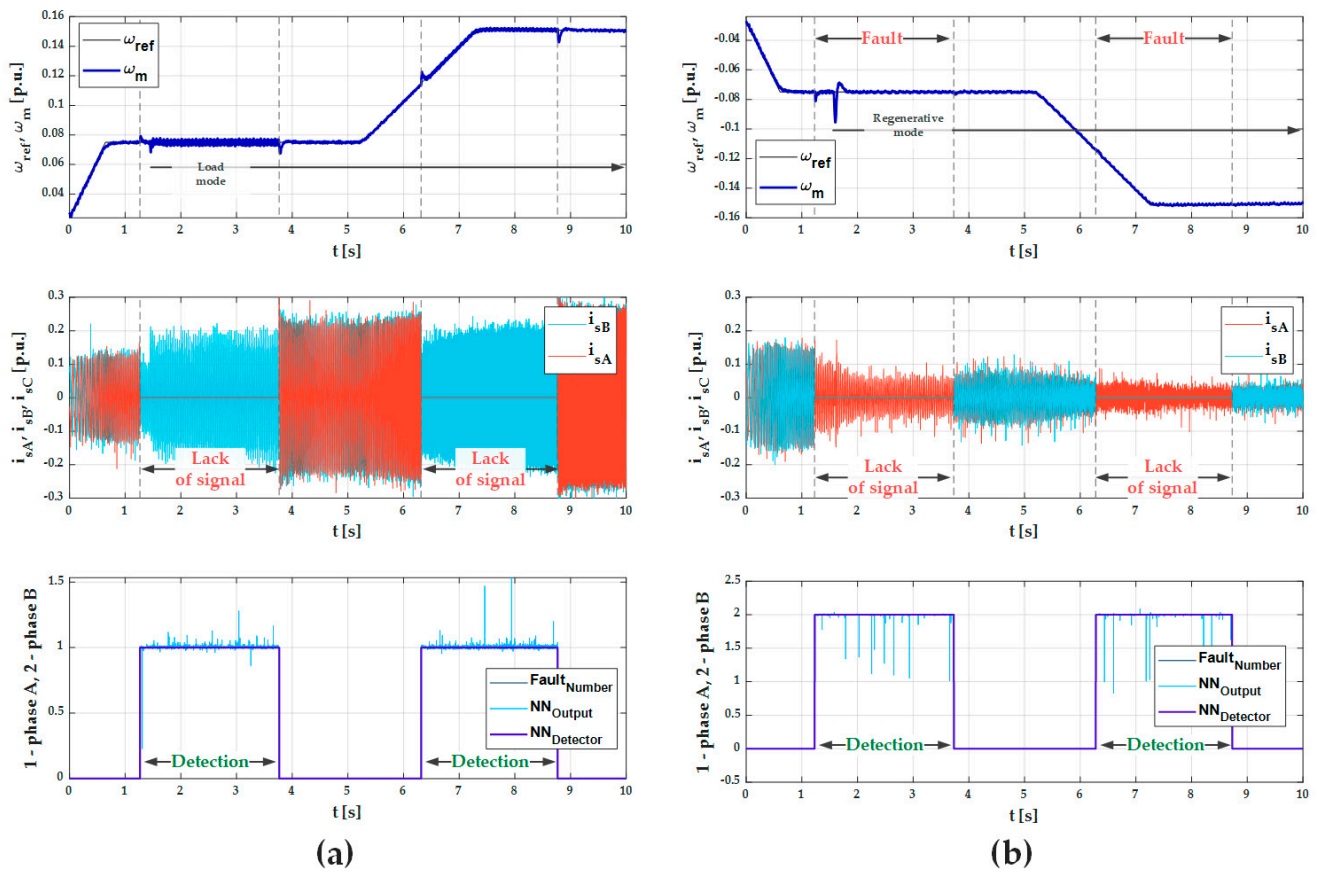


Figure 14. Transients of speed, stator currents, and detector response during lack of signal in phase A in load mode (0.2 TN) (a) and lack of signal in phase B in regenerative mode (0.2 TN) (b).

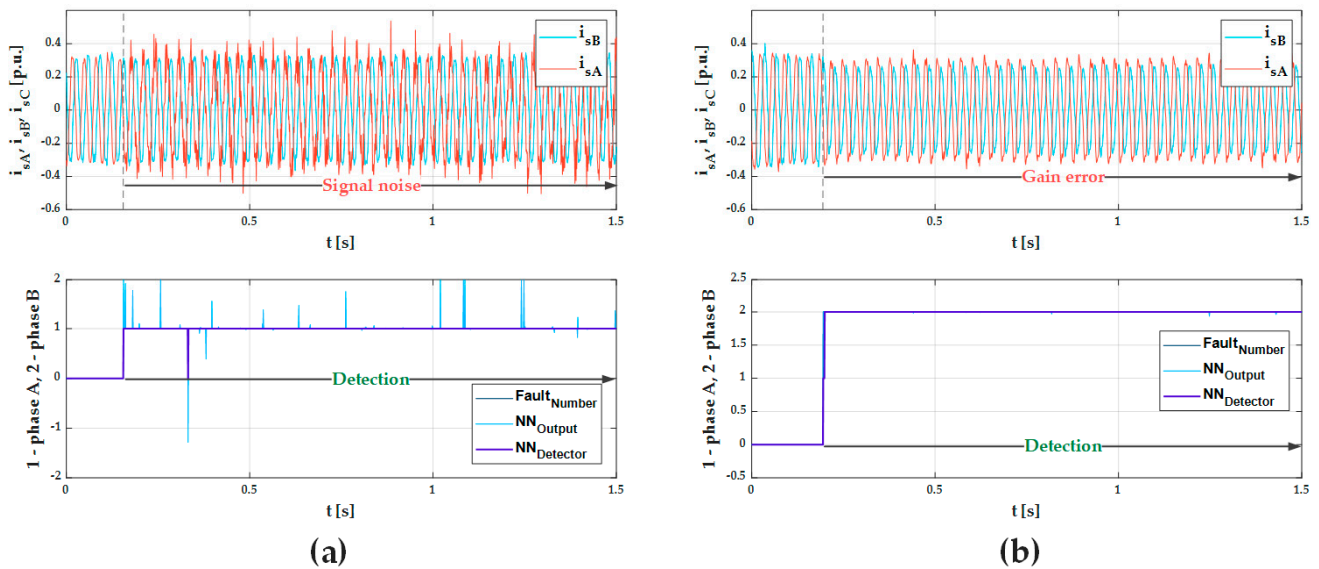


Figure 15. Stator currents and detector response during signal noise in phase A with load (0.2 TN) (a) and gain error in phase B with load (0.2 TN) (b).

In the case of damage detection, time is of the essence. Therefore, the average detection times (time from failure occurrence to its detection) of individual failures in phases A and B, obtained based on the online detection data for the 15-10-1 structure, are presented in Table 8. The raw signal of the neural network detected the failure in the same sample in

which it occurred. The detector response had a delay due to the use of the average of the current sample and the two previous samples. For this reason, the lowest detection time was the duration of two samples—2 ms. In addition, every 10th sample was recorded during the measurements.

Table 8. Detection times.

Type of Fault	Phase A	Phase B
Signal loss	2 ms	4 ms
Gain error	2 ms	4 ms
Signal noise	2 ms	4 ms

The transients showing the detection times for phase A and phase B for various faults are shown in Figure 16. The figure also shows the transients of the fault trigger signal. All signals are presented as a staircase graph. Therefore, in this paper the detection time was shorter than in the papers presented in the introduction.

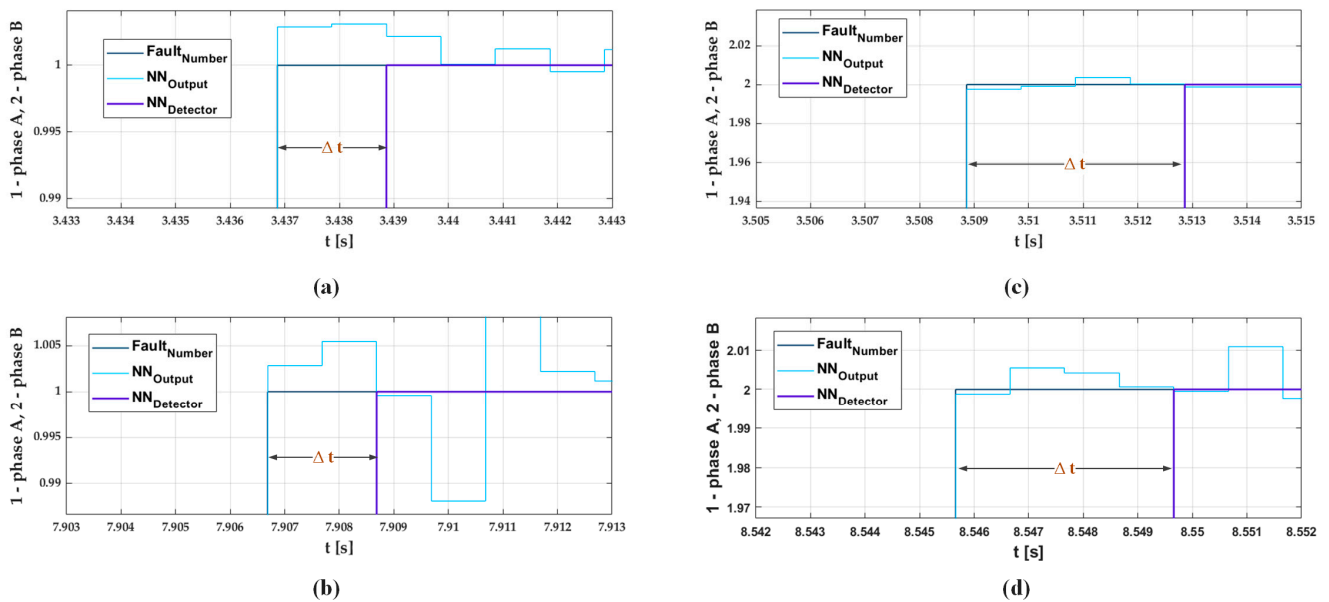


Figure 16. Detection times for signal loss (a) and signal noise (c) in phase A; signal loss (b) and gain error (d) in phase B.

The basis of the FTC system is fault detection and location. Classification of damage is a secondary matter, but it allows to determine how significant the impact on the control structure may fault have. The next part of the work shows the possibilities of using MLP in the classification of damage to current sensors in the PMSM drive system. The classifier has two outputs. The first determines the damage in phase A, and the second in phase B. In this case, it was necessary to use the structure of a neural network with a larger number of neurons in the first hidden layer. The principle of neural network theory was applied here, stating that the number of neurons in the first hidden layer should be twice the number of inputs. Training and testing for the classifier were performed on the same data as for the fault detector, excluding the regenerative mode. Therefore, in the case of the classifier, the results for the 30-10-2 structure are presented. The efficiency of the classifier is shown in Figure 17. The results for both inputs are presented separately.



Figure 17. Confusion matrixes with percentage results for training and testing data for tested structure 30-10-2 for Output1(phase A) (a,b) and Output2(phase B) (c,d) in experimental studies.

The transients during online detection, as in the case of the fault detector for the classifier, are shown in Figure 18. The sample transients show the operation of the classifier during signal loss and signal noise in phase A and phase B. The presented results confirmed the efficiency of the classifier in the no-load and the load mode. In this case, also switching on failures in dynamic states did not interfere with the correct classification. In the case of the classifier, both during no-load and load mode, oscillations appeared on the raw network output, even during signal loss. As in any of the previous cases, most errors occur during measurement noise.

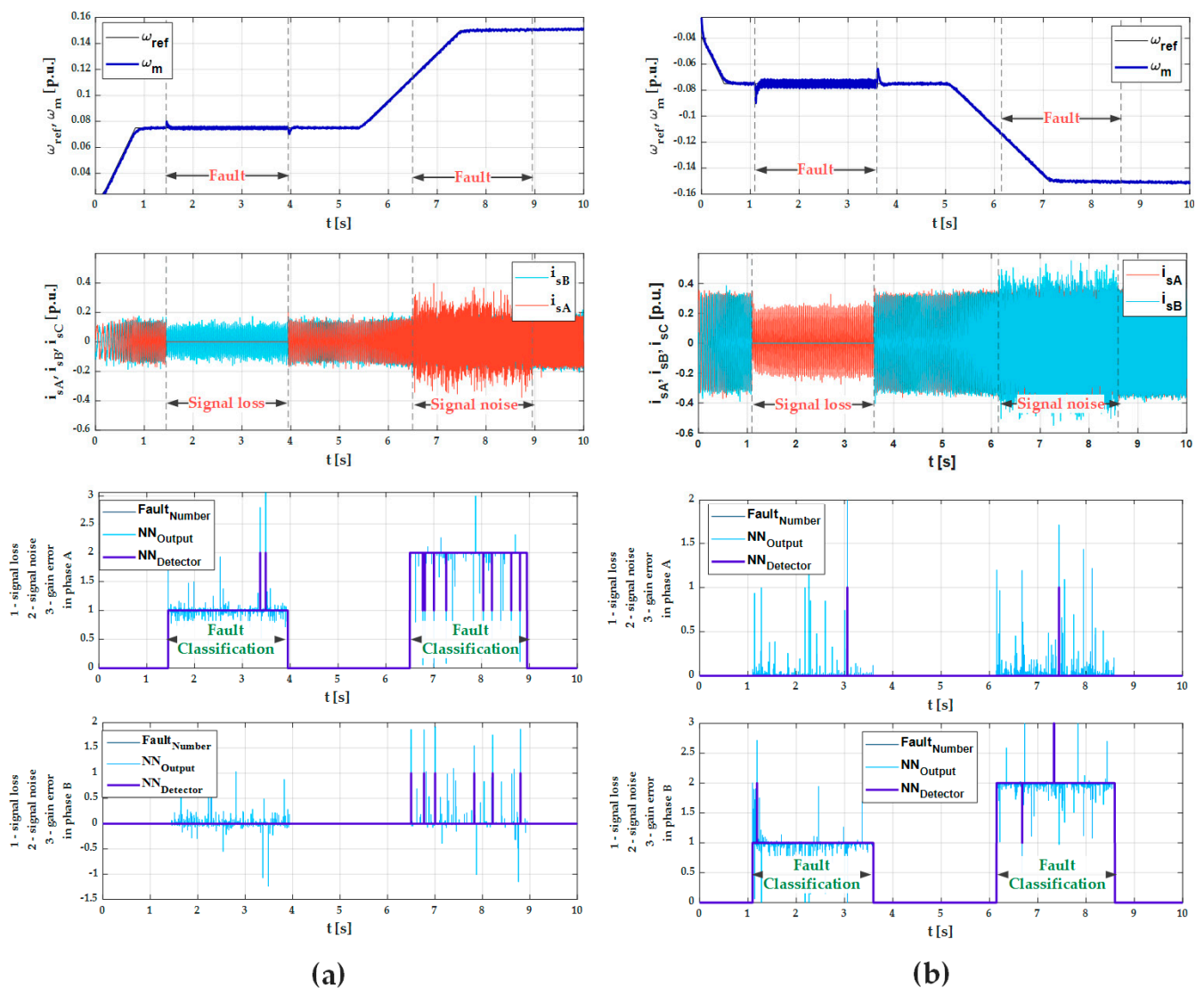


Figure 18. Transients of speed, stator currents, and detector’s Output1 and Output2 during lack of signal and signal noise in phase A without load (a); in phase B in lode mode (0.2 TN) (b).

6. Conclusions

The article presents a neural fault detector of current sensors in the PMSM control system in simulation and experimental studies. Simulation and experimental results are similar. The obtained experimental results testify to the effectiveness of the proposed solution. The presented analysis confirms the following advantages of the application:

- high detection efficiency (100%) and failure location (>99%);
- short detection time, compared to existing solutions, 2–4 ms;
- correct operation in no-load, loaded, and regenerative mode;
- effective detection in stable and dynamic states;
- effective detection, location, and classification of damage without the necessity of compensation;
- the use of raw signals easily available in the control structure as inputs of the neural network;
- low complexity of the implemented network in the control structure;
- the possibility of using it in a system with damage compensation (failure location);
- the use of only two current sensors in the control structure.

In addition to damage detection, the article also presents the possibility of their classification using MLP. The obtained results show that the network correctly recognizes faults. The classification efficiency reaches about 98%. Damage classification may provide additional data for the FTC system. The article presents a detector that can be successfully used in FTC systems; this will be the next step for the authors of the publication.

Author Contributions: Conceptualization, M.D. and K.J.; methodology, M.D. and K.J.; software, K.J.; validation, M.D. and K.J.; formal analysis, M.D. and K.J.; investigation, M.D. and K.J.; resources, M.D. and K.J.; data curation, K.J.; writing—original draft preparation, K.J.; writing—review and editing, M.D.; visualization, K.J.; supervision, M.D.; project administration, M.D.; funding acquisition, M.D. All authors have read and agreed to the published version of the manuscript.

Funding: This research was supported by statutory funds of the Faculty of Electrical Engineering, Wrocław University of Science and Technology (2023).

Data Availability Statement: Not applicable.

Conflicts of Interest: The authors declare no conflict of interest.

References

1. Shen, Q.; Yue, C.; Goh, C.H.; Wang, D. Active Fault-Tolerant Control System Design for Spacecraft Attitude Maneuvers with Actuator Saturation and Faults. *IEEE Trans. Ind. Electron.* **2019**, *66*, 3763–3772. [[CrossRef](#)]
2. Wang, G.; Hao, X.; Zhao, N.; Zhang, G.; Xu, D. Current Sensor Fault-Tolerant Control Strategy for Encoderless PMSM Drives Based on Single Sliding Mode Observer. *IEEE Trans. Transp. Electrification*. **2020**, *6*, 679–689. [[CrossRef](#)]
3. Orłowska-Kowalska, T.; Wolkiewicz, M.; Pietrzak, P.; Skowron, M.; Ewert, P.; Tarchala, G.; Krzysztofiak, M.; Kowalski, C.T. Fault Diagnosis and Fault-Tolerant Control of PMSM Drives—State of the Art and Future Challenges. *IEEE Access* **2022**, *10*, 59979–60024. [[CrossRef](#)]
4. Wu, C.; Guo, C.; Xie, Z.; Ni, F.; Liu, H. A Signal-Based Fault Detection and Tolerance Control Method of Current Sensor for PMSM Drive. *IEEE Trans. Ind. Electron.* **2018**, *65*, 9646–9657. [[CrossRef](#)]
5. Pietrzak, P.; Wolkiewicz, M.; Orłowska-Kowalska, T. PMSM Stator Winding Fault Detection and Classification Based on Bispectrum Analysis and Convolutional Neural Network. *IEEE Trans. Ind. Electron.* **2022**, *70*, 5192–5202. [[CrossRef](#)]
6. Wang, X.; Lu, S.; Huang, W.; Wang, Q.; Zhang, S.; Xia, M. Efficient Data Reduction at the Edge of Industrial Internet of Things for PMSM Bearing Fault Diagnosis. *IEEE Trans. Instrum. Meas.* **2021**, *70*, 3508612. [[CrossRef](#)]
7. Wagner, T.; Sommer, S. Bearing fault detection using deep neural network and weighted ensemble learning for multiple motor phase current sources. In Proceedings of the 2020 International Conference on Innovations in Intelligent Systems and Applications (INISTA), Novi Sad, Serbia, 24–26 August 2020; pp. 1–7. [[CrossRef](#)]
8. Siddiqui, K.M.; Bakhsh, F.I.; Ahmad, R.; Solanki, V. Advanced Signal Processing Based Condition Monitoring of PMSM for Stator-inter Turn Fault. In Proceedings of the 2021 IEEE 8th Uttar Pradesh Section International Conference on Electrical, Electronics and Computer Engineering (UPCON), Dehradun, India, 11–13 November 2021; pp. 1–4.
9. Pham, M.T.; Kim, J.-M.; Kim, C.H. Deep Learning-Based Bearing Fault Diagnosis Method for Embedded Systems. *Sensors* **2020**, *20*, 6886. [[CrossRef](#)]
10. Wang, K.; Zhao, W.; Xu, A.; Zeng, P.; Yang, S. One-Dimensional Multi-Scale Domain Adaptive Network for Bearing-Fault Diagnosis under Varying Working Conditions. *Sensors* **2020**, *20*, 6039. [[CrossRef](#)]
11. Huang, G.; Fukushima, E.F.; She, J.; Zhang, C. Current Sensor Fault Diagnosis Based on Sliding Mode Observer for Permanent Magnet Synchronous Traction Motor. In Proceedings of the 2018 IEEE 27th International Symposium on Industrial Electronics (ISIE), Cairns, Australia, 13–15 June 2018; pp. 835–840. [[CrossRef](#)]
12. Yu, Y.; Wang, Z.; Xu, D.; Zhou, T.; Xu, R. Speed and Current Sensor Fault Detection and Isolation Based on Adaptive Observers for IM Drives. *J. Power Electron.* **2014**, *14*, 967–979. [[CrossRef](#)]
13. Bensalem, Y.; Kouzou, A.; Abbassi, R.; Jerbi, H.; Kennel, R.; Abdelrahem, M. Sliding-Mode-Based Current and Speed Sensors Fault Diagnosis for Five-Phase PMSM. *Energies* **2022**, *15*, 71. [[CrossRef](#)]
14. Li, H.; Qian, Y.; Asgarpour, S.; Sharif, H. PMSM Current Sensor FDI Based on DC Link Current Estimation. In Proceedings of the IEEE 88th Vehicular Technology Conference (VTC-Fall), Chicago, IL, USA, 27–30 August 2018; pp. 1–5.
15. Wang, X.; Wang, Z.; Xu, Z.; Cheng, M.; Wang, W.; Hu, Y. Comprehensive Diagnosis and Tolerance Strategies for Electrical Faults and Sensor Faults in Dual Three-Phase PMSM Drives. *IEEE Trans. Power Electron.* **2019**, *34*, 6669–6684. [[CrossRef](#)]
16. Mehta, H.; Thakar, U.; Joshi, V.; Rathod, K.; Kurulkar, P. Hall sensor fault detection and fault tolerant control of PMSM drive system. In Proceedings of the 2015 International Conference on Industrial Instrumentation and Control (ICIC), Pune, India, 28–30 May 2015; pp. 624–629.

17. El Khil, S.K.; Jlassi, I.; Estima, J.O.; Mrabet-Bellaaj, N.; Cardoso, A.J.M. Detection and isolation of open-switch and current sensor faults in PMSM drives, through stator current analysis. In Proceedings of the 2017 IEEE 11th International Symposium on Diagnostics for Electrical Machines, Power Electronics and Drives (SDEMPED), Tinos, Greece, 29 August–1 September 2017; pp. 373–379. [\[CrossRef\]](#)
18. El Khil, S.K.; Jlassi, I.; Estima, J.; Mrabet-Bellaaj, N.; Cardoso, A.M. Current sensor fault detection and isolation method for PMSM drives, using average normalised currents. *Electron. Lett.* **2016**, *52*, 1434–1436. [\[CrossRef\]](#)
19. Li, H.; Qian, Y.; Asgarpoor, S.; Sharif, H. Machine Current Sensor FDI Strategy in PMSMs. *IEEE Access* **2019**, *7*, 158575–158583. [\[CrossRef\]](#)
20. Li, H.; Qian, Y.; Asgarpoor, S.; Sharif, H. A Sensor Fault Isolation Scheme for Co-existence of PMSM Current Sensor and Non-sensor Imbalance Faults. In Proceedings of the 2019 IEEE Applied Power Electronics Conference and Exposition (APEC), Anaheim, CA, USA, 17–21 March 2019; pp. 2608–2613. [\[CrossRef\]](#)
21. Zhang, G.; Wang, G.; Zhou, H.; Li, C.; Wang, G.; Xu, D. Current Sensor Fault Diagnosis and Fault-Tolerant Control for Encoderless PMSM Drives Based on Dual Sliding-Mode Observers. In Proceedings of the 2019 IEEE Applied Power Electronics Conference and Exposition (APEC), Anaheim, CA, USA, 17–21 March 2019; pp. 2549–2553. [\[CrossRef\]](#)
22. Foo, G.H.B.; Zhang, X.; Vilathgamuwa, D.M. A Sensor Fault Detection and Isolation Method in Interior Permanent-Magnet Synchronous Motor Drives Based on an Extended Kalman Filter. *IEEE Trans. Ind. Electron.* **2013**, *60*, 3485–3495. [\[CrossRef\]](#)
23. Nademi, H.; Hoosh, B.M.; Norum, L. A nonlinear observer-based fault tolerant concept in IPMSM drive. In Proceedings of the XIX International Conference on Electrical Machines—ICEM, Rome, Italy, 6–8 September 2010; pp. 1–6. [\[CrossRef\]](#)
24. Adamczyk, M.; Orłowska-Kowalska, T. Influence of Parameter Uncertainty to Stator Current Reconstruction Using Modified Luenberger Observer for Current Sensor Fault-Tolerant Induction Motor Drive. *Sensors* **2022**, *22*, 9813. [\[CrossRef\]](#)
25. Klimkowski, K.; Dybkowski, M. Neural network approach for stator current sensor fault detection and isolation for vector controlled induction motor drive. In Proceedings of the 2016 IEEE International Power Electronics and Motion Control Conference (PEMC), Varna, Bulgaria, 25–28 September 2016; pp. 1072–1078. [\[CrossRef\]](#)
26. Dybkowski, M.; Klimkowski, K. Artificial Neural Network Application for Current Sensors Fault Detection in the Vector Controlled Induction Motor Drive. *Sensors* **2019**, *19*, 571. [\[CrossRef\]](#)
27. Skowron, M.; Teler, K.; Adamczyk, M.; Orłowska-Kowalska, T. Classification of Single Current Sensor Failures in Fault-Tolerant Induction Motor Drive Using Neural Network Approach. *Energies* **2022**, *15*, 6646. [\[CrossRef\]](#)
28. Jankowska, K.; Dybkowski, M. Design and Analysis of Current Sensor Fault Detection Mechanisms for PMSM Drives Based on Neural Networks. *Designs* **2022**, *6*, 18. [\[CrossRef\]](#)
29. Ewert, P.; Orłowska-Kowalska, T.; Jankowska, K. Effectiveness Analysis of PMSM Motor Rolling Bearing Fault Detectors Based on Vibration Analysis and Shallow Neural Networks. *Energies* **2021**, *14*, 712. [\[CrossRef\]](#)
30. Hoai, H.-K.; Chen, S.-C.; Than, H. Realization of the Sensorless Permanent Magnet Synchronous Motor Drive Control System with an Intelligent Controller. *Electronics* **2020**, *9*, 365. [\[CrossRef\]](#)
31. Lu, W.; Keyhani, A.; Fardoun, A. Neural network-based modeling and parameter identification of switched reluctance motors. *IEEE Trans. Energy Convers.* **2003**, *18*, 284–290. [\[CrossRef\]](#)
32. Brandstetter, P.; Kuchar, M. Sensorless control of variable speed induction motor drive using RBF neural network. *J. Appl. Log.* **2017**, *24*, 97–108. [\[CrossRef\]](#)
33. Shen, T.; Kilic, A.; Thulfaut, C.; Reuss, H. An Intelligent Diagnostic Method for Permanent Magnet Synchronous Motors (PMSM) in the Electric Drive of Autonomous Vehicles. In Proceedings of the 2019 21st European Conference on Power Electronics and Applications (EPE'19 ECCE Europe), Genova, Italy, 3–5 September 2019.
34. Moosavi, S.; Djerdir, A.; Ait-Amirat, Y.; Khaburi, D. ANN based fault diagnosis of permanent magnet synchronous motor under stator windingshorted turn. *Electr. Power Syst. Res.* **2015**, *125*, 67–82. [\[CrossRef\]](#)
35. Nyanteh, Y.; Edrington, C.; Srivastava, S.; Cartes, D. Application of Artificial Intelligence to Real-Time Fault Detection in Permanent Magnet Synchronous Machines. *IEEE Trans. Ind. Appl.* **2013**, *49*, 1205–1214. [\[CrossRef\]](#)
36. Guimarães, C.J.B.V.; Fernandes, M.A.C. Real-time Neural Networks Implementation Proposal for Microcontrollers. *Electronics* **2020**, *9*, 1597. [\[CrossRef\]](#)
37. Saoud, L.S.; Khellaf, A. A neural network based on an inexpensive eight-bit microcontroller. *Neural Comput. Appl.* **2011**, *20*, 329–334. [\[CrossRef\]](#)
38. Malarczyk, M.; Zychlewicz, M.; Stanislawski, R.; Kaminski, M. Low-Cost Implementation of an Adaptive Neural Network Controller for a Drive with an Elastic Shaft. *Signals* **2023**, *4*, 56–72. [\[CrossRef\]](#)
39. Bishop, M.C. *Neural Networks for Pattern Recognition*, 1st ed.; Oxford University Press: New York, NY, USA, 1996.
40. Haykin, S. *Neural Networks, A Comprehensive Foundation*; Macmillan College Publishing Company: New York, NY, USA, 1994.
41. Yu, H.; Wilamowski, B.M. Levenberg–Marquardt Training. In *Industrial Electronics Handbook*, 2nd ed.; Chapter 12, Intelligent Systems; CRC Press: Boca Raton, FL, USA, 2011; Volume 5, pp. 12–15.

42. *SimPowerSystems Toolbox Users' Manual*, Version 5.2; MathWorks Corp.: Sydney, Australia, 2010.
43. Demuth, H.; Beale, M. *Neural Network Toolbox—User's Guide*, Version 4; The MathWorks, Inc.: Natick, MA, USA, 2004.

Disclaimer/Publisher's Note: The statements, opinions and data contained in all publications are solely those of the individual author(s) and contributor(s) and not of MDPI and/or the editor(s). MDPI and/or the editor(s) disclaim responsibility for any injury to people or property resulting from any ideas, methods, instructions or products referred to in the content.